Numerical study of an optically pumped multimode D$_2$O laser

K. Sasaki[a)]
Department of Electronics, Nagoya University, Nagoya 464-01, Japan

T. Tsukishima
Department of Electronics, Aichi Institute of Technology, Toyota, Aichi 470-03, Japan

A numerical simulation of an optically pumped, multimode D$_2$O laser was carried out based on Lamb's semiclassical laser theory. The numerical code includes the dispersion effect of the laser medium (D$_2$O gas in the cavity) in order to simulate the strength of mode coupling accurately. As a result, multiple-longitudinal-mode oscillations around the Raman resonance frequency were obtained that are roughly in agreement with experimental observations. Energy spectra of the D$_2$O laser emission obtained by the simulation were compared with those of the experimental results for various D$_2$O gas pressures. By including the dispersion effect, temporal variations of mode frequencies were calculated. In addition, resonant pumping was examined to obtain spectrally narrow outputs by tuning a frequency of a pump CO$_2$ laser pulse to the line center of the absorption band of D$_2$O molecules. © *1997 American Institute of Physics.* [S0021-8979(97)03801-2]

I. INTRODUCTION

Spectrally narrow outputs are required in many applications of optically pumped far-infrared (FIR) lasers. For example, ion temperature measurements of high-temperature fusion plasmas by collective scattering of laser light[1] need a megawatt class FIR radiation with a narrow spectral width ($\Delta f < 50$ MHz) and a long pulse duration ($\tau > 1$ μs).[2] However, in most high-power FIR lasers, several cavity eigenmodes oscillate simultaneously since the gain bandwidth produced by optical pumping is broader than the longitudinal mode spacing, resulting in a broad spectral width of the output radiation.[3,4]

We have developed an optically pumped high-power (200 kW) D$_2$O laser at a wavelength of 385 μm with the intention of applying it to ion temperature measurements of high-temperature plasmas, and have measured the emission spectra with a high frequency resolution less than a few megahertz.[4] As a result, multiple-longitudinal-mode oscillations were also observed in our D$_2$O laser. The present numerical work was motivated by the experimental observations of complex spectral characteristics of our optically pumped D$_2$O laser. Detailed understanding about the spectral characteristics is necessary since spectral narrowing of the D$_2$O laser is a key issue for application to the ion temperature measurements.[5,6]

The theoretical study of optically pumped FIR lasers was pioneered by Panock and Temkin.[7] They calculated spectral profiles of small signal gain produced by optical pumping with the density matrix formalism. The variation of the small signal gain profile by the ac Stark effect for a strong pump field was shown in their work. Okada *et al.* developed a rate equation code and utilized it for a design of a D$_2$O laser.[8] In that code, the gain for temporally varying pump and D$_2$O laser fields was calculated by the theory of Panock and Temkin. Theoretical studies of FIR lasers including the above two works were restricted to the single-mode treat-ment until 1983, since it was difficult to solve the equations of motion for the density matrix elements in the presence of multiple longitudinal modes.

However, the multimode treatment is inevitable to investigate spectral characteristics of FIR lasers since they usually oscillate with multiple longitudinal modes. In 1984, Dupertuis *et al.* developed the Fourier expansion method, in which the gains of multiple longitudinal modes were calculated simultaneously.[9] They adopted that method to investigate cross-saturation characteristics of the gain and discussed single-mode stability.[10] After that, we adopted the Fourier expansion method to simulate the temporal evolution of a multimode D$_2$O laser.[11,12] As a result, agreement with the experimental results was obtained on the output power characteristics. However, there were great discrepancies with the experimental observations of the spectral characteristics, that is, the number of significantly excited longitudinal modes was smaller than the experimental results. The discrepancies were thought to be due to the fact that the dispersion effect in the laser medium was neglected and mode spacings were equalized in the Fourier expansion method.[9] The equal mode spacings may cause strong coupling among the longitudinal modes, resulting in the smaller number of the oscillation modes.

Inclusion of the dispersion effect (variations of mode frequencies from the resonance frequencies of the empty cavity) may thus be necessary to obtain numerical results that are consistent with the experimental observations. In the present simulation, we adopted Lamb's semiclassical laser theory[13] to include the dispersion effect of the D$_2$O laser medium. Temporal variations of the amplitudes and frequencies of 21 longitudinal modes were calculated. The equations of motion for the density matrix elements were solved by a numerical method. As a result, multiple-longitudinal-mode oscillation was obtained by the simulation that roughly agreed with the experimental results.[14]
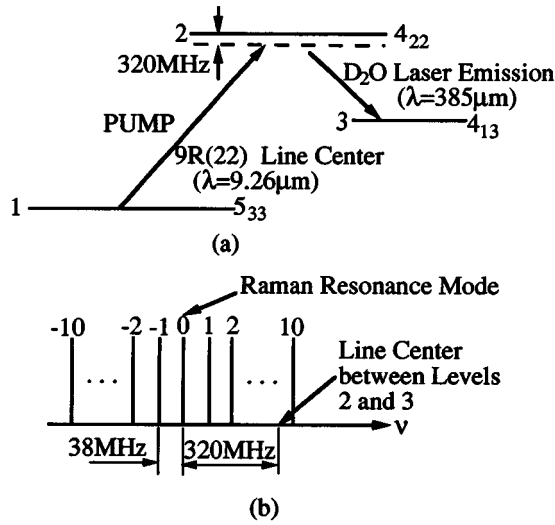
a)Electronic mail: sasaki@nuee.nagoya-u.ac.jp

(a)

Raman Resonance Mode

(b)

FIG. 1. (a) Energy diagram of the D_2O molecule considered in the present simulation, (b) configuration of the assumed 21 longitudinal modes.

II. MODEL OF THE SIMULATION

In Lamb's semiclassical laser theory,[13] the interaction between the laser medium and classical electromagnetic fields is analyzed by making use of the density matrix formalism. The polarization induced in the laser medium is calculated by solving the equations of motion for the density matrix elements. For optically pumped D_2O lasers, a simple three-level system illustrated in Fig. 1(a) provides an accurate enough approximation for calculating the polarization.[15] The classical electromagnetic field consists of a pump CO_2 laser field $E_{pump}(z,t)$ and a FIR field $E_{FIR}(z,t)$ generated by the D_2O laser, namely,

$$E(z,t) = E_{pump}(z,t) + E_{FIR}(z,t). \qquad (1)$$

For linearly polarized fields, scalar values can be used for the electric fields. In the present simulation, transverse effects of the cavity were neglected and the pump and D_2O laser fields were assumed to be constant over the cross section of the D_2O laser since the pump field used in the experiments had a roughly uniform spatial distribution and no higher-order transverse modes were observed in the D_2O laser emission. However, laser instabilities induced by the transverse effects have been predicted by a theory,[16] and could possibly affect the emission spectrum of the D_2O laser. The pump field was assumed to be monochromatic at the line center of the 9R(22) transition line of CO_2 molecules as follows:

$$E_{pump}(z,t) = \tfrac{1}{2} E_p(t) \exp[-i(\Omega t - Kz)] + \text{c.c.}, \qquad (2)$$

which is a consistent condition with our experiment. It couples to the absorption band between levels 1 and 2, and pumps D_2O molecules to level 2 in Fig. 1(a). The frequency of the pump field Ω is approximately 320 MHz lower than the resonance frequency between levels 1 and 2. The amplitude of the pump field $E_p(t)$ was assumed to have no spatial variations along the optical axis.

The FIR field generated by the D_2O laser is obtained via the stimulated Raman transition between levels 2 and 3 since
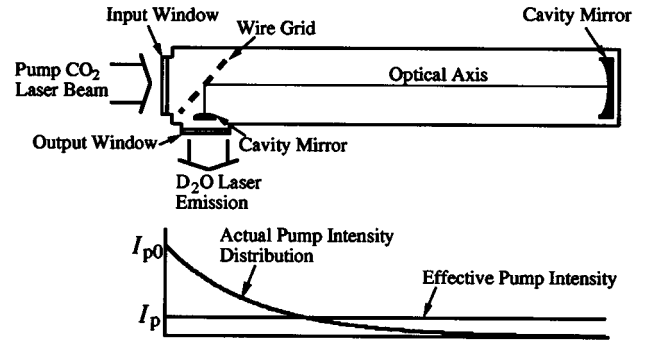

FIG. 2. Schematic of a D_2O laser cavity of the usual type and the corresponding spatial distribution of the pump intensity.

the frequency of the pump field is not resonant between levels 1 and 2. In the present simulation, 21 longitudinal modes were assumed around the Raman resonance frequency (320 MHz lower than the resonance frequency between levels 2 and 3) with spacings for the empty cavity of 38 MHz as shown in Fig. 1(b). The FIR field was expressed as

$$E_{FIR}(z,t) = \frac{1}{2}\sum_{n=-10}^{10} E_n(t)\exp[-i\{\nu_n t - k_n z + \phi_n(t)\}] + \text{c.c.}, \qquad (3)$$

where a ring resonator was assumed for the sake of simplicity instead of the Fabry-Perot cavity used in the experiments.

The equations of motion for the density matrix elements under both the slowly varying envelope approximation and the rotating wave approximation are readily obtained as follows for the above three-level system and electric fields, provided that the Doppler effect by the thermal motion of D_2O gas is neglected.[10] The width of the pressure broadening is much larger than the Doppler width in the FIR wavelength range for usual operating gas pressures. The equations are

$$\dot{\tilde{\rho}}_{11} = \Gamma_1(n_1^0 - \tilde{\rho}_{11}) - 2\,\text{Im}[\alpha^* \tilde{\rho}_{21}], \qquad (4)$$

$$\dot{\tilde{\rho}}_{22} = \Gamma_2(n_2^0 - \tilde{\rho}_{22}) + 2\,\text{Im}[\alpha^* \tilde{\rho}_{21} + \beta^* \tilde{\rho}_{23}], \qquad (5)$$

$$\dot{\tilde{\rho}}_{33} = \Gamma_3(n_3^0 - \tilde{\rho}_{33}) - 2\,\text{Im}[\beta^* \tilde{\rho}_{23}], \qquad (6)$$

$$\dot{\tilde{\rho}}_{21} = -(\gamma_{21} + i\Delta_{21})\tilde{\rho}_{21} - i\alpha(\tilde{\rho}_{22} - \tilde{\rho}_{11}) + i\beta\tilde{\rho}_{31}, \qquad (7)$$

$$\dot{\tilde{\rho}}_{23} = -(\gamma_{23} + i\Delta_{23})\tilde{\rho}_{23} - i\beta(\tilde{\rho}_{22} - \tilde{\rho}_{33}) + i\alpha\tilde{\rho}_{31}^*, \qquad (8)$$

$$\dot{\tilde{\rho}}_{31} = -(\gamma_{31} + i\Delta_{31})\tilde{\rho}_{31} - i\alpha\tilde{\rho}_{23}^* + i\beta^*\tilde{\rho}_{21}, \qquad (9)$$

where $\tilde{\rho}_{ij}$ is the slowly varying amplitude of the density matrix element ρ_{ij} defined by

$$\rho_{ii}(z,t) = \tilde{\rho}_{ii}(z,t), \qquad (10)$$

$$\rho_{21}(z,t) = \tilde{\rho}_{21}(z,t)\exp[-i(\Omega t - Kz)], \qquad (11)$$

$$\rho_{23}(z,t) = \tilde{\rho}_{23}(z,t)\exp[-i(\nu_0 t - k_0 z)], \qquad (12)$$

$$\rho_{31}(z,t) = \tilde{\rho}_{31}(z,t)\exp[-i\{(\Omega - \nu_0)t - (K - k_0)z\}], \qquad (13)$$

K. Sasaki and T. Tsukishima

TABLE I. Various parameters used in the present numerical simulation.

Quantities	Symbols	Values	Units
Dipole moment	μ_{12}	1.08×10^{-31}	C m
	μ_{23}	2.27×10^{-30}	C m
Longitudinal relaxation rate	Γ_i	40×10^6	$\sec^{-1}$ $Torr^{-1}$
Transverse relaxation rate	γ_{ij}	40×10^6	$\sec^{-1}$ $Torr^{-1}$
Population density	N	$3.54 \times 10^{16} \times p$	cm^{-3}
		(p: D_2O gas pressure in Torr)	
Detuning frequency	Δ_{21}	320	MHz
	Δ_{23}	320	MHz
Mode spacing of the empty cavity	δ	38	MHz
Quality factor of the cavity	Q	9.3×10^4	–
Amplitudes of the initial electric fields	$\frac{1}{2} c \epsilon_0 E_n(0)^2$	1	$\mu W/cm^2$
Phases of the initial electric fields	$\phi_n(0)$	Random numbers	rad

where n_i^0 stands for the value of ρ_{ii} when no electric fields interact, Γ_i and γ_{ij} are the longitudinal and transverse relaxation constants, respectively, and Δ_{ij} denotes the detuning from the line center frequency given by

$$\Delta_{21} = \omega_{21} - \Omega, \tag{14}$$

$$\Delta_{23} = \omega_{23} - \nu_0, \tag{15}$$

$$\Delta_{31} = \Delta_{21} - \Delta_{23} = \omega_{31} - \Omega + \nu_0, \tag{16}$$

with ω_{ij} being the resonance frequency between levels i and j. The Rabi frequencies corresponding to the pump and D_2O laser field amplitudes are given by

$$\alpha(t) = \frac{1}{2\hbar} \mu_{21} E_p(t), \tag{17}$$

$$\beta(z,t) = \frac{1}{2\hbar} \mu_{23} \sum_{n=-10}^{10} E_n(t) \exp[-i\{(\nu_n - \nu_0)t + (k_n - k_0)z + \phi_n(t)\}], \tag{18}$$

where $\hbar$ denotes the Planck constant divided by 2π and μ_{ij} is the dipole moment between levels i and j. Equations (4)–(9) are first order differential equations with respect to time t, while the space coordinate z along the optical axis of the cavity is regarded as a parameter.

On the other hand, temporal behaviors of the slowly varying amplitude $E_n(t)$ and the phase $\phi_n(t)$ of the electric field of mode n are subject to the following well-known equations:[13]

$$\dot{E}_n(t) + \frac{\nu_0}{2Q} E_n(t) = -\frac{\nu_0}{2\epsilon_0} \text{Im}[P_n(t)], \tag{19}$$

$$\nu_n + \dot{\phi}_n(t) = \Omega_n - \frac{\nu_0}{2\epsilon_0} \frac{\text{Re}[P_n(t)]}{E_n(t)}, \tag{20}$$

where Q is the quality factor of the cavity, Ω_n stands for the resonance frequency of the empty cavity for mode n, and ϵ_0 is the permittivity of vacuum. In the simulation, Eqs. (19) and (20) are solved numerically together with Eqs. (4)–(9) at
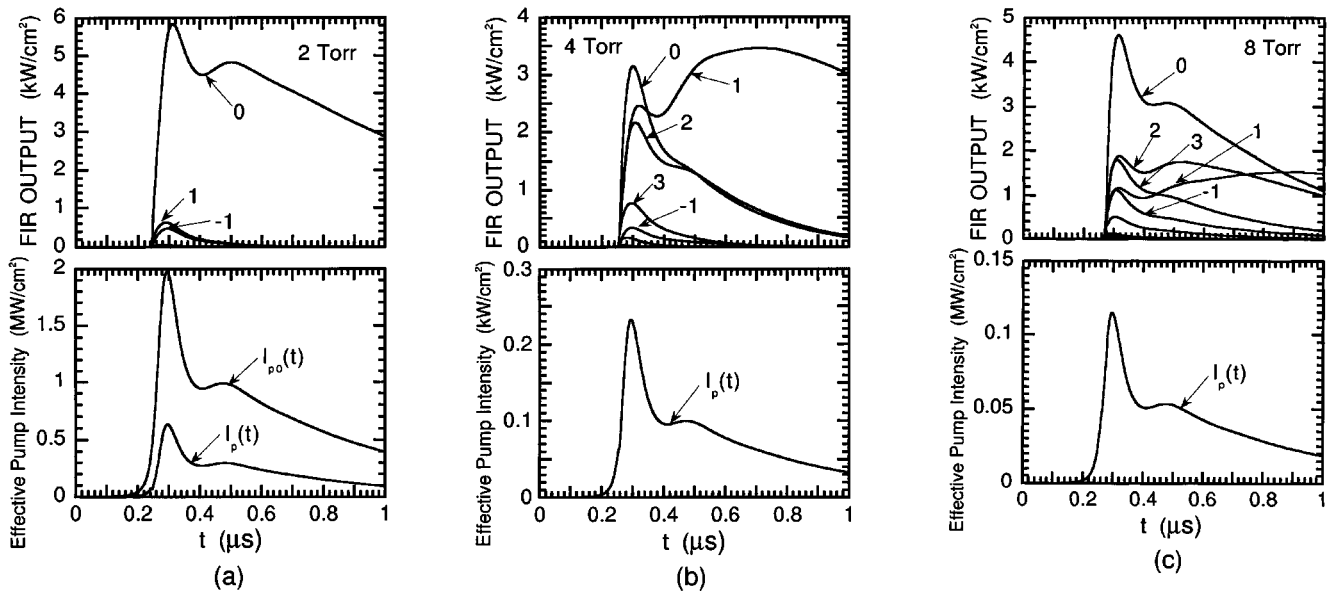

FIG. 3. Temporal variations of mode intensities obtained from the D_2O laser and the corresponding effective pump intensity for D_2O gas pressures of (a) 2 Torr, (b) 4 Torr, and (c) 8 Torr. The wave form of the pump CO_2 laser pulse $I_{p0}(t)$ at the input window is also shown in (a). In the figures showing the D_2O laser outputs, the mode numbers shown in Fig. 1(b) are indicated by arrows.
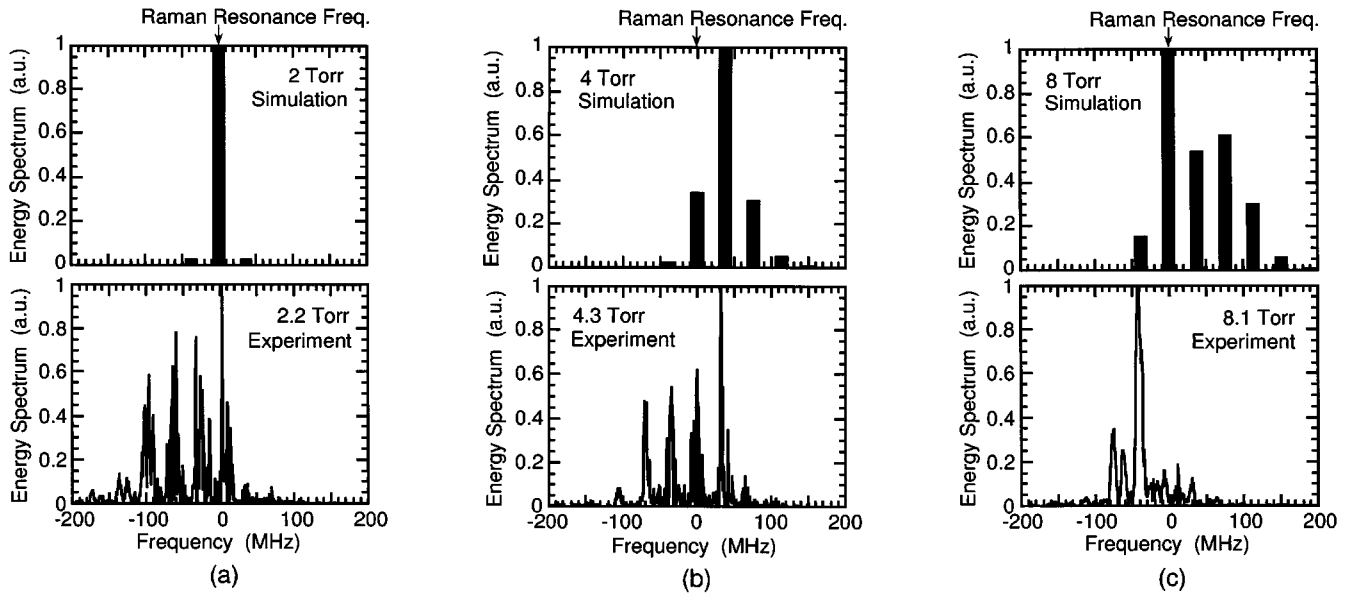
     K. Sasaki and T. Tsukishima

FIG. 4. Comparison of the emission energy spectra of the D_2O laser between the simulation and experimental results for three different D_2O gas pressures.

250 points (250 z values) on the optical axis. The well-known Runge-Kutta integration method was used for the numerical calculation. The macroscopic polarization $P_n(t)$ in Eqs. (19) and (20) can be calculated from the density matrix element $\widetilde{\rho}_{23}$ by the following equation:[13]

$$P_n(t) = \frac{2}{L} N\mu_{23} \exp[i\{(\nu_n - \nu_0)t + \phi_n(t)\}]$$

$$\times \int_0^L \widetilde{\rho}_{23}(z,t) \exp\left(i \cdot 2n\pi \cdot \frac{z}{L}\right) dz, \quad (21)$$

where N represents the sum of population densities of the three energy levels, and L is the roundtrip cavity length.

In order to simulate the actual pumping condition, a temporally varying pump field that was generated by solving the well-known rate equations for transversely excited atmosphere (TEA) CO_2 lasers for the case with injection seeding[17] was used. In usual D_2O lasers, the pump CO_2 laser beam is launched into the D_2O laser along the optical axis of the cavity through an input window located at one end of the cavity. Accordingly, the intensity of the pump field is attenuated as it propagates in the laser medium and has a spatial distribution inside the cavity as shown in Fig. 2. To simplify the calculation, it is assumed here that all the D_2O gas in the cavity is excited uniformly by the effective pump intensity defined by[8]

$$I_p(t) = I_{p0}(t)[\exp\{G_p(t)L\} - 1]/G_p(t)L, \quad (22)$$

where $I_{p0}(t)$ is the pump intensity at the input window. The $I_p(t)$ is the spatially averaged value of the pump intensity inside the cavity. The absorption coefficient $G_p(t)$ in Eq. (22) is calculated from the density matrix element $\widetilde{\rho}_{12}(z,t)$ by

$$G_p(t) = -\frac{2N\Omega\mu_{21}}{\epsilon_0 c L E_p(t)} \text{Im}\left[\int_0^L \widetilde{\rho}_{21}(z,t)dz\right], \quad (23)$$

where c denotes the speed of light. If we do not employ the effective pump intensity, the density matrix element $\widetilde{\rho}_{23}(z,t)$ has a spatial distribution induced by the spatially varying pump intensity. In this case, since the scale length of the spatial distribution of $\widetilde{\rho}_{23}(z,t)$ is similar to the wavelengths of the beat notes in the cavity, the macroscopic polarization $P_n(t)$ cannot be obtained by the projected calculation shown in Eq. (21). To include the spatial distribution of the pump intensity, the real electric fields have to be treated instead of the beat notes, resulting in a long computational time that is not able to be executed with existing computers.

Various parameters used in the simulation are listed in Table I. These values were determined by referring to those given in literature.[15,18] The longitudinal mode spacing and the quality factor of the cavity were chosen to be consistent with our experimental conditions.[4] An unstable resonator with a magnification factor of 4 (the output coupling coefficient is 0.75) is assumed for the quality factor. However, the real geometry of the cavity such as the focusing effects of mirrors was not taken into account in the simulation. Neglect of the focusing effect is not a problem for the pump field since it was dumped in front of the end mirror after the single-pass propagation in the experiments,[4] whereas for the D_2O laser field, there is a possibility that the focusing effects of the cavity mirrors cause the transverse effects and affect the emission spectrum. The initial amplitude of the electric field $E_n(0)$, which acts as the seed for the temporal buildup, is set to be a noise level for all modes, while the initial phase of the electric field $\phi_n(0)$ is given by uniform random numbers generated by a computer between 0 and 2π.

III. RESULTS AND DISCUSSION

A. Temporal behavior of longitudinal modes and energy spectra

In Fig. 3, temporal variations of the longitudinal modes of the D_2O laser are shown for various D_2O gas pressures

together with the corresponding effective pump intensities. The pump CO_2 laser pulse at the input window $I_{p0}(t)$ is also shown in Fig. 3(a). The intensity and pulse shape of $I_{p0}(t)$ were consistent with our experimental condition.[4] The effective pump intensity was reasonably smaller for a higher gas pressure since absorption by D_2O gas in the cavity is stronger for a higher gas pressure. In the figures showing the D_2O laser outputs, the mode numbers shown in Fig. 1(b) are indicated by arrows. Mode 0 has the Raman resonance frequency. The multiple-longitudinal-mode oscillations were obtained by numerical simulation for the first time as shown in Fig. 3. Considering the fact that the Fourier expansion method resulted mainly in single-mode oscillation,[11,12] the inclusion of the dispersion effect is of great importance for the numerical study of multimode D_2O lasers. The significantly excited longitudinal modes were located around the Raman resonance frequency, and the longitudinal modes around the line center did not grow. Similar simulation results were obtained even when the frequency of mode 0 was detuned slightly ($< \delta/2$) from the Raman resonance frequency. For a gas pressure of 2 Torr, the number of the excited modes is smallest, and a roughly symmetric spectral distribution with respect to the Raman resonance frequency was obtained. For gas pressures of 4 and 8 Torr, broadband oscillations around the Raman resonance frequency were observed. The most strongly excited mode shifts from mode 0 to mode 1 at $t \simeq 350$ ns for a gas pressure of 4 Torr. Spontaneous spectral narrowing was observed for all gas pressures. The spectral width at the beginning of the output pulse was broader than that of the tail part. The energy conversion efficiency from the pump to the D_2O laser field was about 0.3%–0.6% for this pressure range, which is a consistent value with our experimental results.[4]

In Fig. 4, energy spectra of the D_2O laser outputs obtained by the simulation were compared with those of the experimental observations.[4] The spectra from the simulation were obtained by integrating the output intensity of each longitudinal mode from 0 to 1 μs. In this simulation, the calculation was ended at 1 μs because of a restriction in the computational time. If the calculation were continued for a longer time, however, the spectrum from the simulation may become slightly narrower for gas pressures of 2 and 4 Torr. The experimental energy spectra were obtained with our heterodyne receiver which had a high frequency resolution of less than 1.3 MHz.[4] In the experiments, multiple-longitudinal-mode oscillations around the Raman resonance frequency were observed for all gas pressures. For a gas pressure of 4 Torr, the spectral distribution from the simulation roughly agreed with the experimental observation, as seen from Fig. 4(b). However, the significantly excited modes in the simulation were located in a slightly higher frequency range than the experimental results. This discrepancy is attributed partly to the assumption of uniform pump intensity. The actual pump field has a strong spatial distribution and is intense around the input window as is illustrated in Fig. 2. The intense pump field induces the ac Stark effect which shifts the peak of the small signal gain profile toward the low frequency side.[7] Hence the experimental spectral distributions were located in the lower frequency range than the
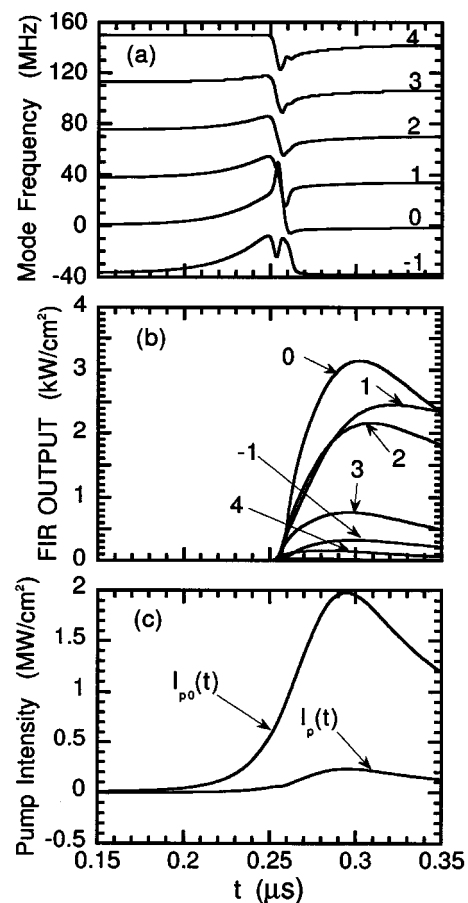

FIG. 5. Temporal variations of mode frequencies (a) for a D_2O gas pressure of 4 Torr together with the mode intensities (b) and the pump filed (c).

simulation results. For gas pressures lower than 2 Torr, spectral widths of the simulation results were narrower than the experimental observations. This discrepancy suggests that Doppler broadening plays an important role in determining the spectral distribution in these low gas pressures. In addition, the assumption of a ring cavity may also be responsible for the discrepancy since the spatial hole burning effect is not included in the ring cavity. If the spatial hole burning effect were taken into consideration, coupling between the longitudinal modes would be weakened,[13] resulting in a broader spectral distribution than the present simulation results. On the other hand, for gas pressures of 6–8 Torr, the spectral distributions from the simulation were broader than those from the experiments. This discrepancy may be related to the fact that the output energy of the D_2O laser obtained in the experiment was considerably weaker than that in the simulation for this pressure range.[4] The gain for the D_2O laser field was larger in the simulation than the experiment, which led the emission spectrum of the simulation to be the broadband distribution. However, it is noted here that the experimental spectral distributions for gas pressures higher than 9 Torr were rather broad[4] and were roughly in agreement with the simulation results except for the location of the peak frequency. When the pump intensity was decreased to 10% of that shown in Fig. 3(a), a slightly narrower spectral distribution with a weak output energy was obtained from the D_2O laser by the simulation. This may be because spectral gain
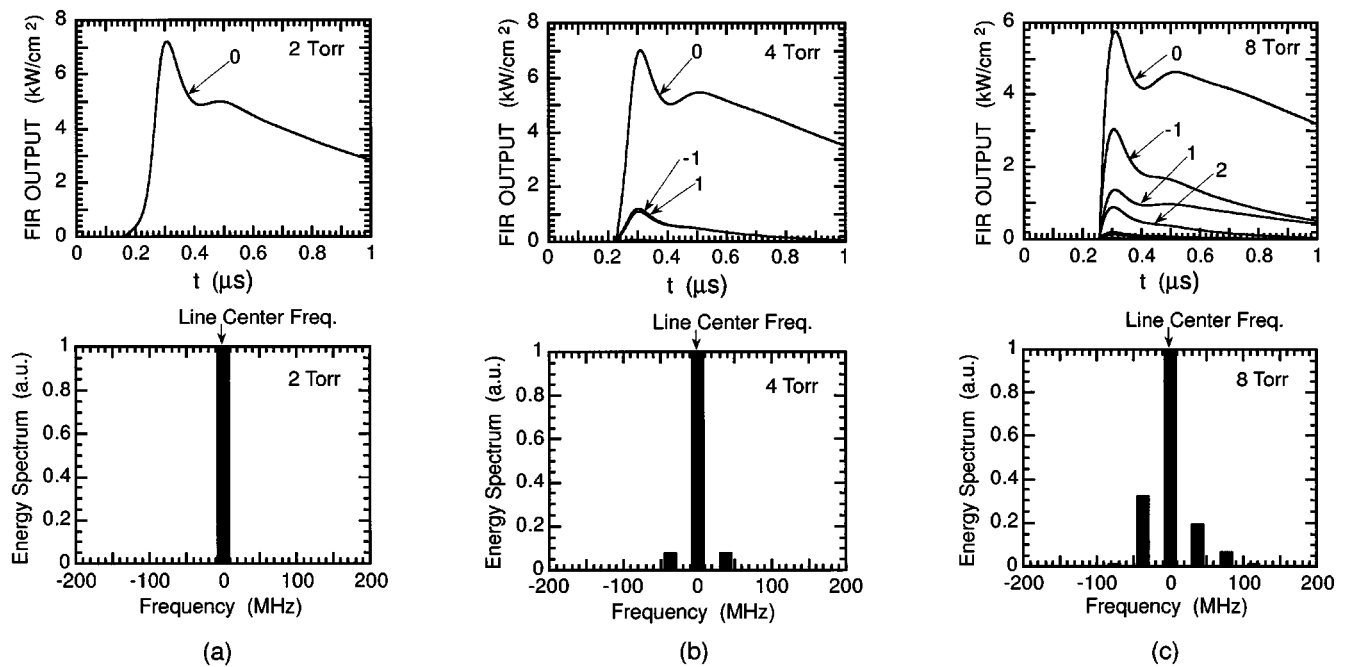
K. Sasaki and T. Tsukishima

FIG. 6. Temporal variations of mode intensities and emission spectra for the case of line-center pumping. The gas pressures are (a) 2 Torr, (b) 4 Torr, and (c) 8 Torr.

broadening due to the ac Stark effect is insignificant for weak pump intensity. The spectrally narrow output for the weak pump intensity was also observed experimentally.[4]

B. Temporal behavior of mode frequencies

As has been described, the inclusion of the dispersion effect of the laser medium (D_2O gas in the cavity) is important to reproduce the multimode oscillation numerically. In fact, when the mode frequencies were fixed at the resonance frequencies of the empty cavity and the mode spacings were equalized, the simulation resulted in single-mode oscillations similar to those obtained by the Fourier expansion method.[11,12] If the laser medium is strongly dispersive, frequency spacings between the longitudinal modes would become different from one another, resulting in the depression of mode coupling. This may explain why the multimode oscillations were obtained in the present simulation.

Figure 5 shows temporal variations of mode frequencies for a gas pressure of 4 Torr during the pulse buildup period. In Fig. 5, the corresponding pump pulse and D_2O laser output are also represented. During the period with a weak pump field ($t \leqslant 0.20 \ \mu s$), the mode frequencies were equal to the resonance frequencies of the empty cavity (mode spacings were 38 MHz). During the evolution of the pump pulse ($0.20 \leqslant t \leqslant 0.25 \ \mu s$), the mode frequencies were pulled toward a frequency around mode 3, where the peak of the small signal gain profile for the effective pump intensity was located. At the oscillation threshold ($0.25 \leqslant t \leqslant 0.265 \ \mu s$), rapid transient phenomena occurred and the mode frequencies returned toward the resonance frequencies of the empty cavity. A mode pushing effect was observed between modes 0 and -1 during this period. After the evolution of the D_2O laser output ($0.265 \leqslant t \leqslant 0.3 \ \mu s$), the mode frequencies varied gradually and reached steady-state values after

$t \simeq 0.3 \ \mu s$. The mode frequencies at the steady state were different from the resonance frequencies of the empty cavity, and the spacings between the modes differed from one another by approximately 1 MHz at $t \simeq 0.3 \ \mu s$.

C. Line-center pumping for spectrally pure operation

The D_2O laser output is obtained by the stimulated Raman transition when the frequency of the pump pulse is detuned from the resonance frequency of the absorption band of D_2O molecules. This off-resonant pumping is usually the case with a TEA CO_2 laser oscillating at the line center of the 9R(22) transition line of CO_2 molecules. However, if the frequency of the pump CO_2 laser pulse is tuned to the resonance frequency of the absorption band of the D_2O molecules (detuned from the line center of 9R(22) by approximately 320 MHz), the D_2O laser output is obtained by so-called laser-like transition and appears around the line center frequency between levels 2 and 3.[19] Tuning the frequency of the pump TEA CO_2 laser can be obtained by inserting a Fabry-Perot etalon inside the cavity and changing the tilting angle of the etalon.[20] In our D_2O laser system, line-center pumping cannot be realized experimentally since an injection-seeded TEA CO_2 laser is employed as the pump source.[4] However, in the simulation, it can easily be examined by setting two parameters such that $\Delta_{12}=0$ and $\Delta_{23}=0$. In this case, mode 0 shown in Fig. 1(b) has the line center frequency.

The energy spectra and the temporal variations of mode intensities for the case of line-center pumping are shown in Fig. 6 for three different D_2O gas pressures. The shape of the pump pulse shown in Fig. 3(a) was adopted again here. Comparing the results by line-center pumping with those by usual off-resonant pumping shown in Figs. 3 and 4, it is clear that the spectral width obtained by line-center pumping was
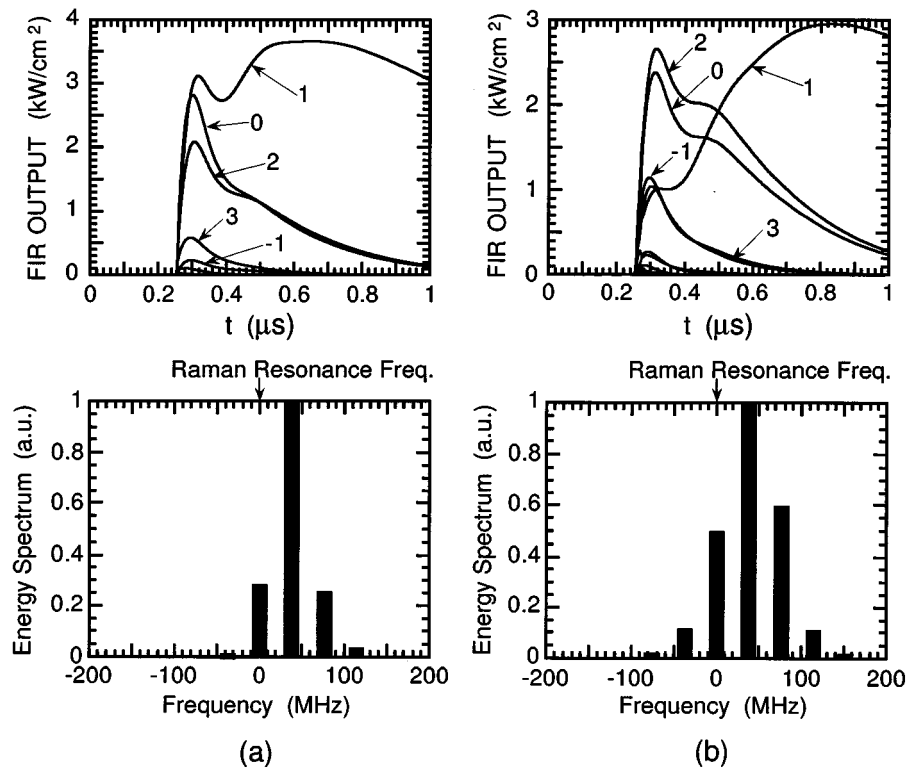
FIG. 7. Temporal variations of mode intensities and emission spectra for two different phases of the initial electric fields. The D_2O gas pressure was 4 Torr.

narrower than that by off-resonant pumping for the same D_2O gas pressure. Spectrally narrow operation is essentially required for D_2O lasers for its application to the ion temperature measurements of high-temperature fusion plasmas. According to the present simulation results, line-center pumping is effective in obtaining spectrally narrow outputs from D_2O lasers without any reduction of the output power. However, considerable effort has to be made to obtain off-line center operation of TEA CO_2 lasers with high stability.

D. Effect of phases of the initial electric fields

In the present simulation, initial amplitudes of the longitudinal modes of the D_2O laser $E_n(0)$ were set to be a noise level, and the initial phases $\phi_n(0)$ were given by uniform random numbers generated by a computer. All the simulation results described above were obtained for the same initial phases and amplitudes of the longitudinal modes. To investigate the effects of the initial electric fields, the simulation was repeated for different initial amplitudes and phases. As a result, the D_2O laser output was not sensitive to the choice of the initial amplitudes corresponding to intensity from 0.1 to 100 $\mu W/cm^2$. However, the simulation results were dependent on the phases of the initial electric fields. Figure 7 shows the energy spectra and the temporal variations of the longitudinal modes obtained for two different phases of the initial electric fields. The D_2O gas pressure was 4 Torr. The phases adopted in Fig. 7 were also different from those used in the other simulations in the present article. Although multiple-longitudinal-mode oscillations around the Raman resonance frequency were obtained for all phases, the energy

spectra and the temporal variations of the mode intensities were dependent on the phases. In the experiments, it was observed that the multimode spectral distributions from the D_2O laser were slightly different from shot to shot for the same operating condition. The present simulation results showing dependence on the initial phases may correspond to the poor shot-to-shot reproducibility of the spectral distribution observed experimentally. If we repeat the calculation for many phases of the initial electric fields and employ the average of the mode spectra for all the gas pressures, we may be able to obtain more general result using the present simulation. However, the conclusions reached in this article deduced from the simulation results with one initial condition are still reliable since each of the mode spectra differs from the average only slightly as seen from Fig. 7.

IV. CONCLUSIONS

In conclusion, we have shown the following.

(i) We have developed a numerical code for an optically pumped multimode D_2O laser. This code is based on Lamb's semiclassical laser theory and includes the dispersion effect of the laser medium (D_2O gas in the cavity).

(ii) Multiple-longitudinal-mode oscillations around the Raman resonance frequency were obtained by the numerical code. The energy spectra from the D_2O laser obtained by the simulation roughly agreed with the experimental observations for a D_2O gas pressures of 4 Torr.

(iii) At the oscillation threshold, rapid variations of the mode frequencies were observed. In the steady state, the frequencies of the longitudinal modes were different from the

resonant frequencies of the empty cavity. These mode frequency characteristics were due to the dispersion effect of D_2O gas in the cavity and were important for obtaining multimode oscillations by the simulation.

(iv) It was predicted by the simulation that spectrally narrow outputs could be obtained from the D_2O laser by tuning the pump pulse frequency to the resonance frequency of the absorption band of D_2O molecules (line-center pumping).

(v) Simulation results were dependent on the initial phases of the longitudinal mode electric fields. This may correspond to the poor shot-to-shot reproducibility of the spectral distribution observed experimentally.

ACKNOWLEDGMENTS

[1] R. Behn, D. Dicken, J. Hackmann, A. S. Salito, M. R. Siegrist, P. A. Krug, I. Kjelberg, B. Duval, B. Joye, and A. Pochelon, Phys. Rev. Lett. **62**, 2836 (1989).

[2] M. R. Green, P. D. Morgan, M. R. Siegrist, and R. L. Watterson, Laboratory Report LRP 168/80, CRPP Ecole Polytechnique Fedérale de Lausanne, Switzerland (1980).

[3] R. Behn, M.-A. Dupertuis, P. A. King, I. Kjelberg, A. S. Salito, and M. R. Siegrist, IEEE J. Quantum Electron. **QE-24**, 549 (1988).

[4] M. Nagatsu, Y. Tsubouchi, N. Takada, K. Sasaki, T. Tsukishima, T. Okada, S. Okajima, K. N. Sato, S. Sudo, and Y. Tsunawaki, Jpn. J. Appl. Phys. **31**, 3873 (1992).

[5] K. Sasaki, N. Takada, O. Takahashi, M. Nagatsu, T. Tsukishima, T. Okada, S. Okajima, Y. Tsunawaki, S. Sudo, K. N. Sato, K. Kondo, H. Arimoto, and K. I. Sato, J. Appl. Phys. **77**, 1378 (1995).

[6] K. Sasaki, O. Takahashi, N. Takada, M. Nagatsu, T. Tsukishima, T. Okada, S. Okajima, Y. Tsunawaki, S. Sudo, K. N. Sato, K. Kondo, H. Arimoto, and K.-I. Sato, Int. J. Infrared Millim. Waves **16**, 2133 (1995).

[7] R. L. Panock and R. J. Temkin, IEEE J. Quantum Electron. **QE-13**, 425 (1977).

[8] T. Okada, R. Behn, M. A. Dupertuis, P. D. Morgan, and M. R. Siegrist, J. Appl. Phys. **54**, 2987 (1983).

[9] M. A. Dupertuis, R. Rainer, E. Salomaa, and M. R. Siegrist, IEEE J. Quantum Electron. **QE-20**, 440 (1984).

[10] M. A. Dupertuis, R. Rainer, E. Salomaa, and M. R. Siegrist, IEEE J. Quantum Electron. **QE-23**, 1217 (1987).

[11] K. Sasaki, K. Matsuoka, M. Nagatsu, and T. Tsukishima, Jpn. J. Appl. Phys. **31**, L1556 (1992).

[12] K. Sasaki, K. Furuhashi, K. Matsuoka, M. Nagatsu, and T. Tsukishima, Rev. Laser Eng. **22**, 116 (1994) (in Japanese).

[13] M. Sargent III, M. O. Scully, and W. E. Lamb, Jr., *Laser Physics* (Addison-Wesley, Reading, MA, 1977).

[14] K. Sasaki, M. Nagatsu, and T. Tsukishima, Opt. Lett. **19**, 1846 (1994).

[15] T. A. DeTemple, in *Infrared and Millimeter Waves*, edited by K. J. Button (Academic, New York, 1979), Vol. 1.

[16] L. A. Lugiato, F. Prati, L. M. Narducci, P. Ru, J. R. Tredicce, and D. K. Bandy, Phys. Rev. A **37**, 3847 (1988).

[17] J. Gilbert, J.-L. Lachambre, F. Rheault, and R. Fortin, Can. J. Phys. **50**, 2523 (1972).

[18] P. Woskoboinikow, W. J. Mulligan, and R. Erickson, IEEE J. Quantum Electron. **QE-19**, 4 (1983).

[19] P. Woskoboinikow, H. C. Praddaude, W. J. Mulligan, D. R. Cohn, and B. Lax, J. Appl. Phys. **50**, 1125 (1979).

[20] Y. Ichikawa, Y. Tsunawaki, M. Yamanaka, S. Okajima, L.-D. Wu, T. Iwasaki, M. Takai, A. Mitsuishi, T. Yamanaka, and C. Yamanaka, Infrared Phys. **27**, 317 (1987).